Revealing the properties of Mn_2Au for antiferromagnetic spintronics

V.M.T.S. Barthem[1], C.V. Colin[2,3], H. Mayaffre[4], M.-H. Julien[4] & D. Givord[1,2,3]

The continuous reduction in size of spintronic devices requires the development of structures, which are insensitive to parasitic external magnetic fields, while preserving the magnetoresistive signals of existing systems based on giant or tunnel magnetoresistance. This could be obtained in tunnel anisotropic magnetoresistance structures incorporating an antiferromagnetic, instead of a ferromagnetic, material. To turn this promising concept into real devices, new magnetic materials with large spin-orbit effects must be identified. Here we demonstrate that Mn_2Au is not a Pauli paramagnet as hitherto believed but an antiferromagnet with Mn moments of $\sim 4\,\mu_B$. The particularly large strength of the exchange interactions leads to an extrapolated Néel temperature well above 1,000 K, so that ground-state magnetic properties are essentially preserved up to room temperature and above. Combined with the existence of a significant in-plane anisotropy, this makes Mn_2Au the most promising material for antiferromagnetic spintronics identified so far.

[1] Instituto de Fisica, Universidade Federal do Rio de Janeiro, Cidade Universitaria, Ilha do Fundao, 21941-972 Rio de Janeiro, Brazil. [2] Univ. of Grenoble Alpes, Institut NEEL, F-38042 Grenoble, France. [3] CNRS, Institut NEEL, F-38042 Grenoble, France. [4] Laboratoire National des Champs Magnétiques Intenses, CNRS-UJF-UPS-INSA, 25 rue des Martyrs, BP166, F-38042 Grenoble 9, France. Correspondence and requests for materials should be addressed to D.G. (email: dominique.givord@grenoble.cnrs.fr).

In a stack including a magnetically ordered material, tunnel anisotropic magnetoresistance (TAMR) represents the variation of resistance across a tunnel barrier, as a function of the angle between the direction of the moments and that of the current (or with respect to a crystallographic direction)[1,2]. A condition for large TAMR is the presence of large spin-orbit (SO) coupling. Magnetoresistive effects in excess of 10% have been obtained with Co/Pt ferromagnetic bilayers, where the SO interaction essentially arises from the noble Pt atoms[2]. The number of ferromagnetic alloys between $3d$ transition metals and noble metals is relatively small, however. The fact that TAMR devices may incorporate an antiferromagnetic (AFM) layer instead of a ferromagnetic one could be exploited in novel spintronic devices[3]. AFM materials being largely insensitive to the effect of an external magnetic field, the parasitic fields that may affect Giant Magnetoresistance (GMR) or Tunnel Magnetoresistance (TMR) nanodevices would not affect TAMR devices. This has stimulated the search for AFM alloys combining high Néel temperature (T_N) and large SO coupling effects[4,5]. Low-temperature (T) magnetoresistive effects in excess of 100% have been obtained in TAMR stacks incorporating AFM MnIr[6].

Mn alloys containing noble metals are often AFM[7,8]. However, this has not been considered to be the case for Mn_2Au. The susceptibility of Mn_2Au is weak ($\chi = 5 \times 10^{-4}$ SI) and almost temperature independent above 50–100 K, which has been taken as a manifestation of Pauli paramagnetism[8]. However, from a first-principles Local Spin Density Approximation (LSDA) study, it was argued that Mn_2Au should be AFM, with a large Mn magnetic moment, approaching $4\mu_B$ per Mn, and a Néel temperature well above room temperature[9]. Subsequently, it was theoretically predicted that the Mn moments are confined in the basal plane of the tetragonal structure of this compound, with a sizeable in-plane anisotropy[3].

In this article, we provide an experimental confirmation of these theoretical predictions, therefore, establishing that Mn_2Au is a particularly promising material for AFM spintronics.

Results

Magnetic susceptibility. The temperature dependence of the experimental magnetization, M_{exp}, measured under an applied field, $\mu_0 H_{app} = 1\,T$, is shown in Fig. 1a. Above 100 K, the derived DC (direct current) susceptibility, χ_{exp} ($= M_{exp}/H_{app}$), is almost temperature independent, amounting to $\chi_{exp} = 5 \times 10^{-4}$ at 300 K. Below typically 100 K, an additional component develops, which is reminiscent of paramagnetic impurities. At low temperatures, a low-field nonlinear term is found for the variation of the magnetization, M_{exp}, under field, obviously due to the same phenomenon leading to the low T increase in susceptibility. From 20 K to room temperature, the isotherm magnetization variation is essentially linear in field up to 7 T (Fig. 1b). At higher temperature, an upturn starts to appear in the variation of the magnetization with applied field (see change of slope above 4 T at 400 K in Fig. 1b). These results, which are in agreement with previous observations, will be analysed in the discussion section, after we have presented data from nuclear magnetic resonance (NMR) and neutron experiments concerning the magnetic structure of Mn_2Au.

Nuclear magnetic resonance. A ^{55}Mn zero-field nuclear magnetic resonance (NMR) spectrum, recorded at room temperature, reveals the existence of five absorption peaks in the frequency range, $v = 186$–195 MHz, as expected for the Zeeman levels of a spin $I = 5/2$ shifted by the quadrupole interaction (Fig. 2). The large intensity of the NMR signal shows that it is representative of the main Mn_2Au phase and not of possible minority phases. Qualitatively, the presence of an NMR signal at such high
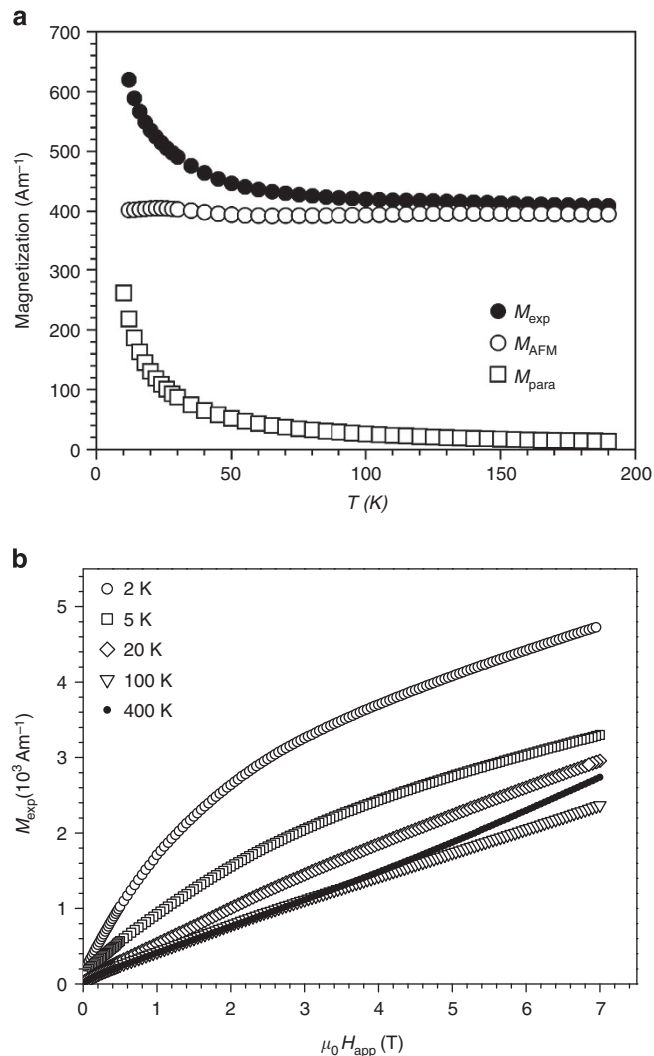
Figure 1 | Magnetic susceptibility measurements. (**a**) Filled circles: Temperature dependence of the experimental magnetization, M_{exp}, measured under $\mu_0 H_{app} = 1\,T$. Squares: Calculated paramagnetic contribution to the magnetization of Mn moments located on Au sites, M_{para} (see text). Open circles: Deduced magnetization, $M_{AFM} = M_{exp} - M_{para}$, representing the antiferromagnetic susceptibility under an applied magnetic field $\mu_0 H_{app} = 1\,T$; (**b**) magnetization, M_{exp}, as a function of the applied magnetic field, $\mu_0 H_{app}$, at temperatures $T = 2, 5, 20, 100$ and 400 K.

frequencies in the absence of any external field demonstrates that ^{55}Mn nuclei experience a large hyperfine internal field, that is, Mn_2Au is magnetically ordered at room temperature. The well-defined lines in the quadrupole-split spectrum and the absence of any additional spectral feature indicate that the spectrum can be modelled by a single site, in agreement with the single crystallographic site of Mn in Mn_2Au: all Mn atoms experience the same hyperfine field, $|H_{hyp}| = v/\gamma^* = 14.3\,MA/m$ ($\gamma^* = \gamma/2\pi = 10.55\,MHzT^{-1}$ is the gyromagnetic ratio), and the same quadrupolar splitting of 0.9 MHz, without any distribution of angles between the principal axes of the magnetic hyperfine and electric field gradient tensors. The relatively large values, for a metallic sample at room temperature, of both the spin–lattice relaxation time T_1 (8 ms) and the spin–spin relaxation time T_2 (314 μs) suggest gapped spin excitations. This is consistent with magnetic order being well established at room temperature.
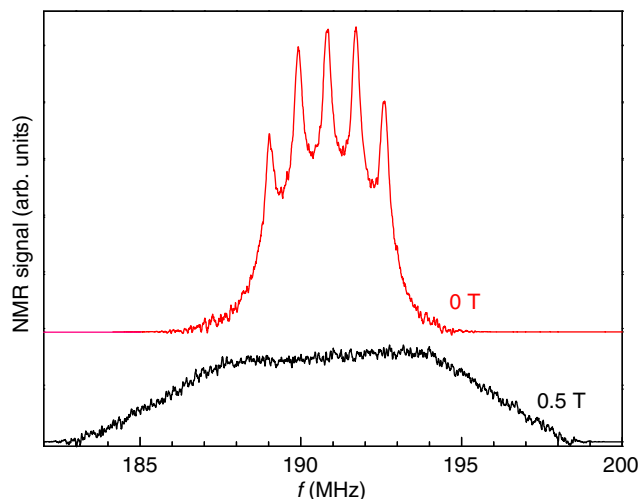
Figure 2 | Room temperature ^{55}Mn NMR spectra of Mn$_2$Au. In red: zero-field spectrum. In black: spectrum under $\mu_0 H_{app} = 0.5$ T.

Applying a magnetic field of $\mu_0 H_{app} = 0.5$ T changes the five-peak spectrum observed in zero-field into an unresolved broad spectrum extending from 183 to 198 MHz (Fig. 2). This effect is typical of AFM systems for which the equivalence of all sites in the constituent grains breaks down with the appearance of a distribution of angles between internal and applied fields[10]. The total field experienced by ^{55}Mn nuclei takes all values between $H_{hyp} + H_{app}$ and $-H_{hyp} + H_{app}$, which explains the additional extension of the spectrum by ~ 4 MHz in both directions.

Magnetic structure determination using neutron diffraction. In order to determine the exact magnetic structure of Mn$_2$Au, a neutron diffraction study was performed on the D1B diffractometer at the Institut Laue-Langevin (Grenoble, France). A neutron wavelength of 1.28 Å was used. Below 900 K, the main peaks of all diffraction patterns are characteristic of the Mn$_2$Au phase (2 K pattern shown in Fig. 3). Small additional peaks are present that can be associated with (i) the nuclear and magnetic peaks of MnAu, which orders antiferromagnetically ($k = 0$ ½ 0) at $T_N = 523$ K, and (ii) a small MnO impurity, not visible in the laboratory X-ray data (method section), having the AFM structure ($k = $ ½ ½ ½) at $T_N = 118$ K. Quantitative Rietveld analysis[11] of the neutron data gave a value of 2.3 weight % MnAu, in excellent agreement with the value derived from X-ray data. The MnO impurity phase amounted to 0.4(1)% (see Fig. 3 and Supplementary Fig. S1). The 2 K pattern was initially analysed under the assumption that no magnetism is present in Mn$_2$Au, that is, only nuclear scattering is involved (Fig. 4a). The diagram calculated within FULPROF displays all experimentally observed reflections[11]. However, at low scattering angles, the experimental intensities of almost all reflections are larger than the calculated ones, and the discrepancy may be larger than the statistical error by up to three orders of magnitude. This suggests the existence of magnetic contributions to the Bragg reflections, with a magnetic structure described in the same cell as the crystallographic one, that is, a propagation vector equal to [000]. This type of order may be described as an intra-unit cell AFM order. The neutron diffraction pattern was thus compared with each of the patterns expected for the magnetic structures allowed by the group theory within the tetragonal structure of Mn$_2$Au. The representational analysis followed the formalism of Bertaut[12], with the SARAh[13] http://www.ccp14.ac.uk, SARAh (2000) programme. The representations were constructed with the m^k Fourier
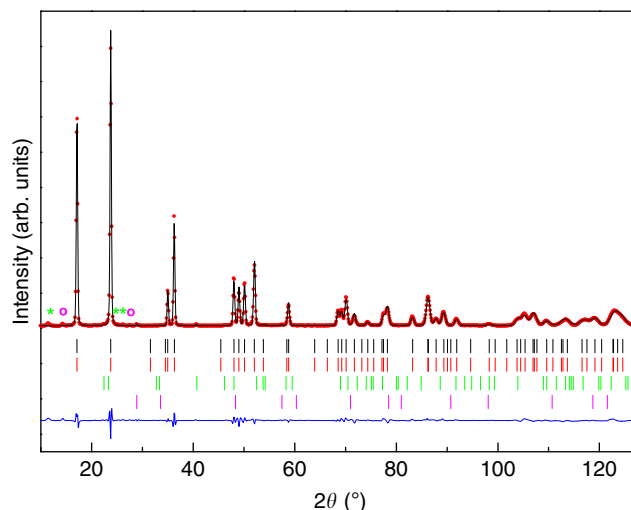

Figure 3 | Mn$_2$Au neutron diffraction pattern recorded at 2 K and optimum fit obtained. Red: experimental data, black: fit to the data corresponding to the Γ10 magnetic structure, faint black line in the lower part of the figure: difference between experiment and fit. Another antiferromagnetic structure is compatible with the group theory, noted Γ2 (see Table 1), but it is incompatible with experimental data (Fig. 4b). Black and red ticks: nuclear and magnetic diffraction peaks of Mn$_2$Au; green ticks: nuclear diffraction peaks revealing the presence of AuMn (impurity amounting to 2.3% of the total sample according to quantitative Rietveld analysis); purple ticks: nuclear diffraction peaks revealing the presence of MnO (impurity amounting to 0.4% of the total sample); green stars: magnetic diffraction peaks associated with the MnAu impurity; purple circles: magnetic diffraction peaks associated with the MnO impurity.

components corresponding to the Mn atoms at the 4e position (0, 0, z). The different basis vectors, which are associated with each irreducible representation, were also calculated. Table 1 gives the four possible magnetic structures, consistent with I 4/mmm symmetry and $k = [000]$, together with the resulting magnetic space group. Two possible magnetic structures, Γ3 and Γ9, can be discarded, as they are ferromagnetic. The two AFM structures (Γ2 and Γ10) were carefully examined. The fit corresponding to the Γ2 structure is shown in Fig. 4b, whereas the one corresponding to Γ10 is shown in Fig. 3. Only the latter is compatible with the experimental data and it corresponds to the [A_x, A_y, 0] basis functions. The resulting magnetic space group is Im'mm. The Mn moments, μ_{Mn}, form ferromagnetic sheets perpendicular to c. Their orientation alternates from one sheet to the next. This structure is identical to that theoretically predicted by Khmelevskyi and Mohn[9]. The moments are confined in the plane perpendicular to the uniaxial axis, c, in agreement with the large intensity of the 00l reflections. Due to the tetragonal symmetry of the Mn$_2$Au crystallographic structure, the neutron analysis does not allow the determination of the direction of the moments within the plane. In the scheme of Fig. 5, the moments within the (001) plane are arbitrarily represented along the [110] basal plane direction (see below). At 2 K, the Mn atoms bear a moment of 4.0(3) μ_B. The refinement converged to a magnetic R-factor value of 2.63. In the whole temperature range, from 2 to 900 K, the analysis provides essentially the same result (Supplementary Table S2). The temperature dependence of the Mn magnetic moment in the whole range of measured temperatures is remarkably weak (Fig. 6). At the highest temperature (900 K), the Mn moment still amounts to approximately 85% of its value at 0 K. Note that the value of the Mn moment in the analysis is strongly correlated to the value

of the B thermal factors. At room temperature, the thermal factors of Au and Mn were fixed at values identical to those determined by X-ray diffraction (B_{iso} in Supplementary Table S1). At the other temperatures, an overall additional B factor was refined (noted B_{ov} in Supplementary Table S2).
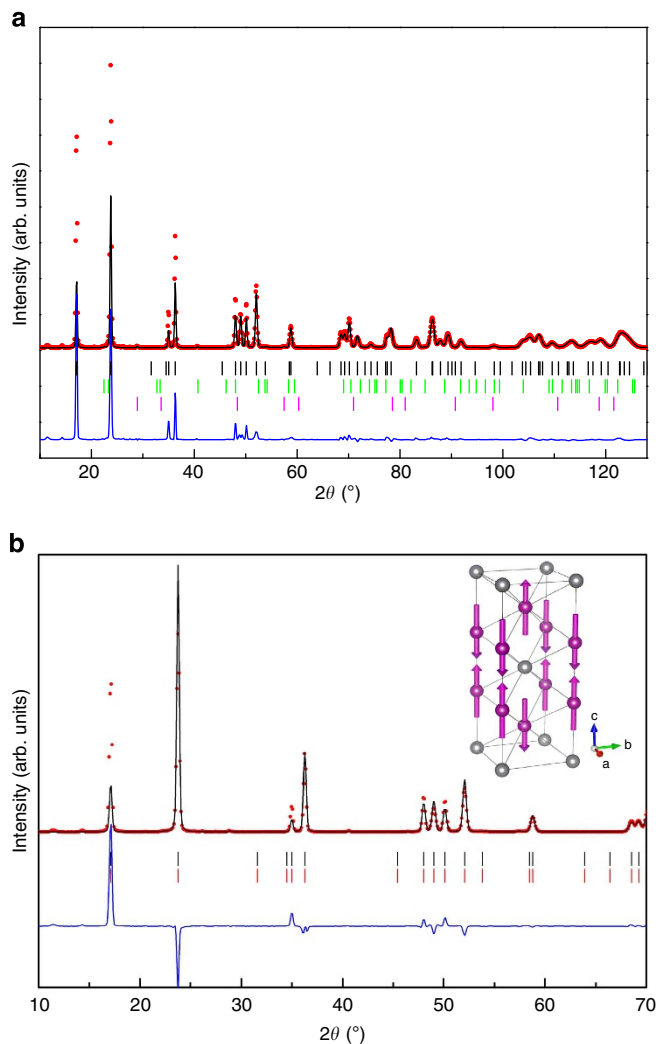

Figure 4 | Other tentative fits to the 2 K neutron diffraction pattern of Mn$_2$Au. (a) Assuming only nuclear scattering; red: experimental data, black: fit to the data assuming only nuclear scattering. The discrepancy (difference pattern in blue) between observed and calculated intensities may reach orders of magnitude. (b) Expected for the antiferromagnetic Γ2 structure; red: experimental data, black: fit to the data, blue: difference between experiment and fit. The large discrepancy at low scattering angles establishes that Γ2 cannot be the real magnetic structure of Mn$_2$Au. Inset: schematic representation of the Γ2 magnetic structure.

Assuming that the temperature dependence of the Mn moment corresponds to that given by the $S = 2$ Brillouin function, a Néel temperature of 1575 (225) K is extrapolated from the present data (see Fig. 6a). As mean field models tend to overestimate magnetic ordering temperatures, this value can be seen as an upper limit for the Néel temperature of Mn$_2$Au. To obtain a more reliable value of T_N, the experimentally determined temperature dependence of the Mn sub-lattice moment in Mn$_2$Au was compared with the temperature dependence found in other AFM Mn compounds with Néel temperatures well above room temperature, namely Mn$_3$Ir ($T_N = 960$ K)[14] and MnPd ($T_N = 535$ K)[15]. For these two compounds, the T/T_N dependence of the reduced intensity of the 100 magnetic Bragg reflection (proportional to the square of the magnetic moment), as measured by neutron diffraction, is shown in Fig. 6b. The value of T_N in Mn$_2$Au was adjusted so that the T/T_N dependence of the square of the Mn magnetic moment resembles those found for Mn$_3$Ir and MnPd. Under such an hypothesis, the T_N value of Mn$_2$Au is found to be in the temperature interval 1,300–1,600 K. Furthermore, the experimental temperature dependence of the sub-lattice Mn moment, $\mu_{Mn}(T)$, in Mn$_2$Au was calculated
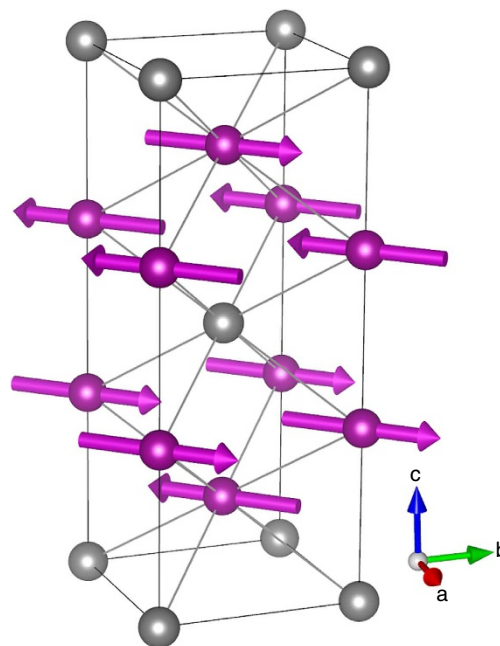

Figure 5 | Magnetic structure of Mn$_2$Au derived from the neutron diffraction study. The Mn moments form ferromagnetic sheets perpendicular to c. Their orientation alternates from one sheet to the next. The moments are confined in the plane perpendicular to the uniaxial axis, c. The neutron analysis does not allow the determination of the direction of the moments within the plane.

Table 1	Possible magnetic structures for Mn$_2$Au.			
Irreducible representation	**Mn position 4e1**	**Mn position 4e2**	**Basis function**	**Magnetic space group**
Γ2	[0,0,w]	[0,0,$-w$]	(0, 0,A_z)	I4/m$m'm'$
Γ3	[0,0,w]	[0,0,w]	(0, 0,F_z)	I4/mmm'
Γ9	[u,v,0]	[u,v,0]	(F_x,F_y,0)	I$m'm'm$
Γ10	**[u,v,0]**	**[$-u$,$-v$,0]**	**(A_x,A_y,0)**	**I$m'mm$**

Magnetic structures consistent with the space group I4/mmm and the propagation vector $k = (0, 0, 0)$. For their description, two Mn atoms in the 4e position must be considered, characterized with 4e_1 = (0, 0, z) and 4e_2 = (0,0, − z) and z = 0.33286. The notations $F = (+ +)$ and $A = (+ −)$ refer to the spin respective orientation following[12]. The structures noted Γ3 and Γ9 are ferromagnetic, the structures noted Γ2 and Γ10 are antiferromagnetic. The magnetic structure Γ10, marked in bold, is the only one in agreement with the neutron data.

according to the phenomenological expression[16] :

$$\mu_{Mn}(T) = \mu_{Mn}(0) \cdot \left(1 - \left(\frac{T}{T_N}\right)^\alpha\right)^\beta \qquad (1)$$

where α and β are parameters. At low temperature, the moment varies as $1 - cT^\alpha$, whereas close to T_N it varies as $[1 - (T/T_N)^\beta]$ (Kuz'min[17] proposed a similar expression to describe the temperature dependence of the spontaneous magnetization in ferromagnetic systems). The parameter values $\alpha = 2$ and $\beta = 0.3$ were taken, corresponding to average values derived from fits of the

temperature dependence of neutron intensities in Mn₃Ir and MnPd. Note that $\alpha = 2$ is the exponent predicted by spin-wave theory in antiferromagnets and $\beta = 0.3$ is close to the 3D Heisenberg critical exponent of 0.33. The, thus, calculated temperature dependence of the manganese moment is compared with the experimental data in Fig. 6c, for T_N equal to 1,300 and 1,600 K, respectively.

The ratio between the Mn magnetic moment value, as deduced from neutron scattering, and the hyperfine field measured by NMR on ⁵⁵Mn gives a hyperfine coupling constant of 5.5 Tμ_B^{-1}. In Mn compounds where the on-site contribution to the hyperfine field dominates, the hyperfine coupling constant is usually of the order of 10–15 Tμ_B^{-1} (ref. 18). The low value found in Mn₂Au might be attributed to a transferred hyperfine field from the nearest Mn neighbours, having a sign opposite to the dominant on-site contribution. Such a large transferred hyperfine field has been found in a number of R-Mn compounds (R = rare-earth)[19].

Discussion

Not only is the magnetic structure of Mn₂Au determined in this study identical to that predicted by first-principles calculations, but also, the value of the Mn magnetic moment, 4.0 (3) μ_B at 2 K, is consistent with the calculated value of 3.64 μ_B and the Néel temperature, evaluated to be in the range of 1,300–1,600 K, which is compatible with the theoretical value of 1,610 K (ref. 9). Introducing SO coupling in a self-consistent second-variational procedure, the magnetocrystalline anisotropy may be evaluated at 0 K using the torque method[3]. It amounts to − 25 K per Mn₂Au (corresponding to a second-order anisotropy constant $K = 7.3 \times 10^6$ J m⁻³), where the negative sign means that the basal plane is favoured with respect to the uniaxial axis. Among metallic AFM alloys, Mn-Ir close to the 3:1 composition is known to have a large magnetocrystalline anisotropy. From the analysis of the blocking temperature of Mn-Ir nanograins, O'Grady et al.[20] have derived that the room temperature second-order anisotropy constant is of the order of 5.5×10^5 J m⁻³. In order to evaluate the room temperature anisotropy in Mn₂Au, one may use the approximate Akulov expression[21], according to which the anisotropy coefficients of order l should vary with temperature as $m^{\frac{l(l+1)}{2}}$, where m is the reduced magnetization. Introducing in this expression the temperature dependence of the sub-lattice magnetization given by Equation (1) above, one derives

Figure 6 | Temperature dependence of the Mn magnetic moment.
(**a**) Temperature dependence of the Mn magnetic moment compared with dependences given by the Brillouin function $S = 2$. Open black dots: experimental Mn magnetic moment derived from the neutron data (The vertical bars are the errors obtained in the quantitative Rietveld analysis of the neutron data.). Calculated temperature dependences for $T_N = 1,575$ K (continuous line), $T_N = 1,350$ K (dotted line) and $T_N = 1,800$ K (dashed line). (**b**) Comparison of the temperature dependence of neutron magnetic intensities in Mn₂Au with temperature dependences found in other antiferromagnetic systems. Open black dots: square of the Mn magnetic moment in Mn₂Au (left scale). The point positions correspond to $T_N = 1,450$ K, whereas the two extremes of the horizontal error bars correspond to $T_N = 1,300$ K and $T_N = 1,600$ K, respectively. In red: T/T_N dependence of the normalized magnetic intensity of the 100 Bragg reflection (expected to be proportional to the square of the Mn magnetic moment) in antiferromagnetic Mn₃Ir (filled circles)[14] and MnPd (open circles)[15]. (**c**) Comparisons of the temperature dependence of the Mn magnetic moment in Mn₂Au with the temperature dependence predicted for the phenomenological expression $\mu_{Mn}(T) = \mu_{Mn}(0) \cdot \left(1 - \left(\frac{T}{T_N}\right)^\alpha\right)^\beta$ (see text). Open black dots: Mn magnetic moment. Calculated temperature dependences of the Mn magnetic moment obtained for $\alpha = 2$, $\beta = 0.3$ and two different assumed values of $T_N = 1,300$ K (dotted line) and 1,600 K (dashed line), respectively.
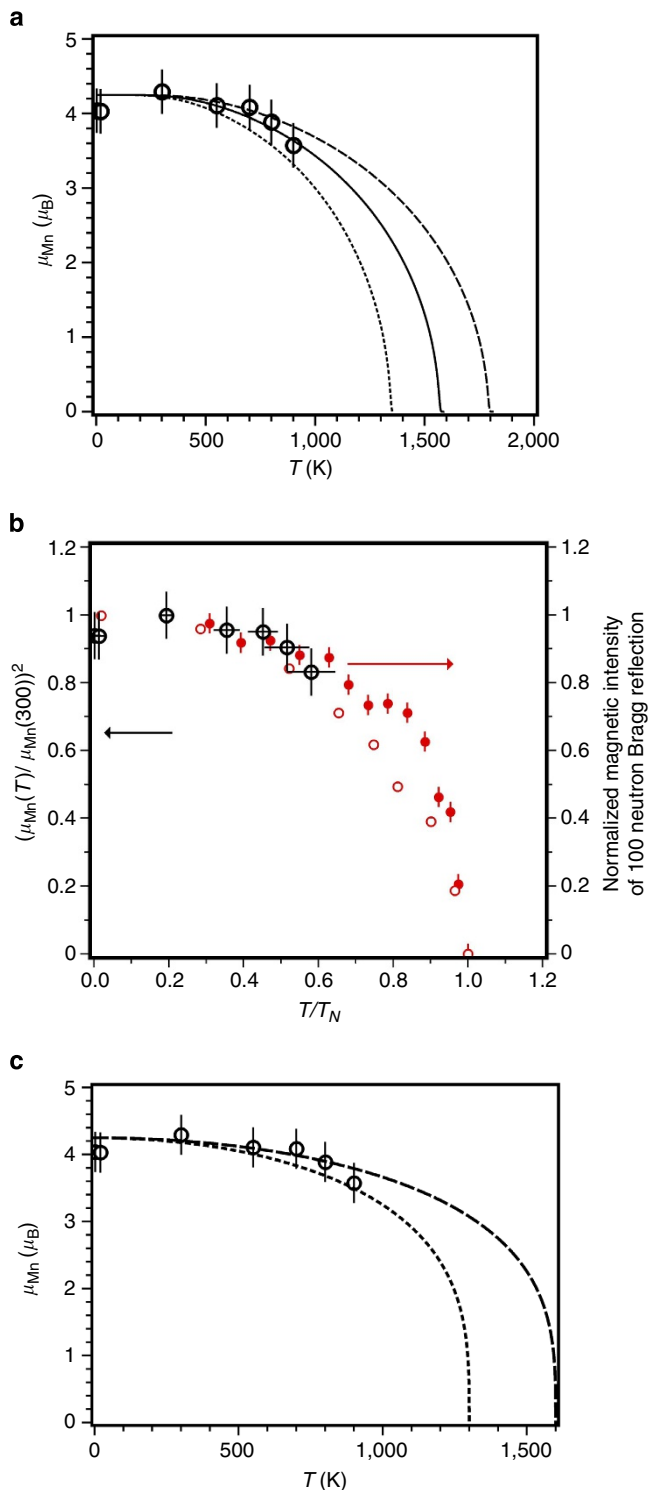
that the second-order anisotropy coefficient at 300 K is of the order of 90% of the 0 K value. The anisotropy in Mn_2Au is thus expected to be at least an order of magnitude higher than in Mn-Ir.

Although not providing a quantitative value for the anisotropy energy, the neutron study is consistent with calculations, in establishing that the Mn moments are in the basal plane of the tetragonal structure. The in-plane fourth-order anisotropy of Mn_2Au is evaluated below. It is much weaker than the here-discussed second-order anisotropy and this constitutes an important element for TAMR.

Having established the existence of an AFM order in Mn_2Au with NMR and neutron studies, we will now analyse the magnetic susceptibility of Fig. 1 within the molecular field model. The magnetic energy, E_m, may be expressed as:

$$E_m = \frac{3}{2}NkT_N = \mu_0 W M_{sl}^2 + \mu_0 W' M_{sl}^2 \qquad (2)$$

where $N = 42 \times 10^{27}\,m^{-3}$ is the number of Mn atoms per unit volume, M_{sl} is the Mn sublattice magnetization, W is the coefficient representing interactions within a given AFM sublattice and W' is the coefficient representing interactions between sublattices. The perpendicular susceptibility, $\chi_\perp$, is equal to $1/W'$. For an isotropic powdered sample, the low-T susceptibility, χ, should be equal to $2/3$ $\chi_\perp$. From $\chi = 5 \times 10^{-4}$ SI and $M_{sl} = 0.78 \times 10^6\,A\,m^{-1}$ (corresponding to $4\,\mu_B$ per Mn), one derives $W' = 1{,}330$. We have no experimental means to evaluate W. The values of the three principal exchange integrals (see Fig. 1 in ref. 9): J_1 (J_1 $k_B^{-1} = -396$ K) and J_2 (J_2 $k_B^{-1} = -532$ K) (representing coupling with Mn moments in the other sub-lattice) and J_3 (J_3 $k_B^{-1} = 115$ K) (characterizing the interaction within a given sub-lattice) were derived in the already mentioned first-principle calculations[9]. Term to term identification gives: $\mu_0 W' M_{sl}^2 = N(4J_1 + J_2)k_B$ and $\mu_0 W\ M_{sl}^2 = N \times 4J_3\ k_B$. Assuming that the ratio between the W values is identical to that derived from the theoretical calculations, gives $W = 290$. The Néel temperature then derived from equation (2) amounts to 1,435 (200) K, a value in agreement with the one derived from the neutron analysis.

In AFM materials, a spin-flop transition may be observed at a field, $H_{sf} \approx \sqrt{2H_{exch}H_A}$, where $H_{exch} = W'M_{sl}$ ($\mu_0 H_{exch} = 1{,}300$ T in Mn_2Au, derived from susceptibility measurements) is the intersublattice exchange field and $H_A = K/\mu_0 M_{sl}$ ($\mu_0 H_A = 10$ T in Mn_2Au, derived from theoretical second-order anisotropy) is the anisotropy field. At H_{sf}, a change in the magnetic susceptibility occurs. In the present case, the spin-flop transition is predicted to occur at $H_{sf} = 123 \times 10^6\,A\,m^{-1}$ ($\mu_0 H_{sf} = 150$ T), a value beyond possible experimental observation. As the Mn moments are confined in the basal plane of the structure, another spin-flop transition may occur due to the in-plane fourth-order anisotropy (difference in energy between the [100] and [110] directions). Attributing to this phenomenon, the change in susceptibility under $\mu_0 H_{app} = 5$ T at $T = 400$ K (Fig. 1b), an in-plane anisotropy field of approximately $\mu_0 H_A = 0.01$ T is deduced. In ref. 3, the calculated 0 K in-plane anisotropy field amounts to 0.04 T. Applying the $m^{\frac{l(l+1)}{2}}$ law for $l = 4$, gives approximately 0.03 T at 400 K, which is of the order of the experimentally determined value. This low in-plane anisotropy energy indicates that TAMR structures based on Mn_2Au could exploit the in-plane rotation of the Mn moments from one easy in-plane direction to the other[3].

The susceptibility increase found in the present study below around 100 K, as well as in the initial study of Mn_2Au[8], may be attributed to 'impurity' Mn atoms occupying the Au site[9]. The exchange coupling on these Mn moments is zero, the different contributions cancelling each other out. χ_{para}, the contribution of such paramagnetic uncoupled moments to the total susceptibility χ_{exp}, was calculated assuming an effective

Mn moment of $4.9\,\mu_B$ (derived from $S = 2$, in agreement with the low-temperature $4\,\mu_B$ Mn moment). The fraction x of Au sites occupied by Mn atoms was determined by imposing that the susceptibility, $\chi_{AFM} = \chi_{exp} - \chi_{para}$, be approximately constant, as expected for an antiferromagnet at low-T (see Fig. 1a, note that in this figure the magnetization in $A\,m^{-1}$ under 1 T is plotted and not the susceptibility, thus the notation M_{exp}, M_{para} and M_{AFM}). The obtained value of x is 0.25% (the exchange-field on the Mn impurity moments due to the canting under field of the normal Mn moments was neglected). This very small value indicates that the atomic order in Mn_2Au is close to perfect. Mn atoms on the Au sites would inevitably introduce undesired frustration. The high value of the Néel temperature in Mn_2Au and the fact that it is close to the theoretical value are additional indications of the quality of the atomic order in this compound.

Ten-nanometre-thick films of Mn_2Au have recently been prepared by molecular beam epitaxy, on top of a 5-nm-thick Fe film, itself grown on (001) MgO (ref. 5). The observation of exchange-bias behaviour provided convincing but indirect evidence of AFM order in Mn_2Au. The present study establishes the AFM nature of this compound unambiguously. The experimentally determined magnetic structure is identical to that theoretically predicted. The Néel temperature is found to be between 1,300 K and 1,600 K, which should be compared with 1,145 K in MnIr and below 500 K in recently discovered CuMnAs (ref. 4). Large magnetoresistance anisotropy requires large SO coupling effects, which, in a uniaxial structure, may lead to the existence of a large magnetocrystalline anisotropy. In case the magnetic moments align along the unique axis, the difficulty in rotating them from the easy axis to the basal plane makes it impossible to exploit TAMR effects. In Mn_2Au, on the contrary, the moments being in the basal plane of the structure, their rotation from one easy in-plane direction to the other may be obtained under the effect of a relatively small external excitation (for example, by coupling to an external applied field, involving the exchange-spring phenomenon as in MnIr(ref. 6)). This provides the mechanism for large TAMR effects as illustrated in Fig. 7. In the absence of SO interactions, the Mn orbitals would take the fourfold basal plane symmetry of the tetragonal structure (Fig. 7a). However, owing to the strong SO coupling resulting from Mn-Au hybridization, the Mn orbitals take a uniaxial symmetry, the principal axis of the electron distribution becoming the moment direction (Fig. 7b,c). Assume a TAMR stack made of two Mn_2Au layers separated by an insulating barrier, the moment direction in one layer being fixed, as in Fig. 7b, for example, whereas in the other it may rotate from (b) to (c). Owing to the anisotropy in
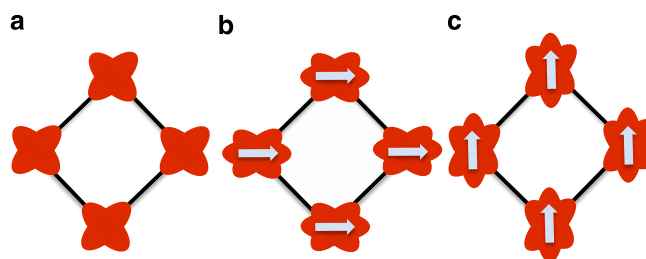

Figure 7 | Illustration of the mechanism by which low-field large TAMR may be expected in Mn_2Au. (**a**) In the absence of spin-orbit interactions, the Mn orbitals (in red) take the fourfold basal plane symmetry of the tetragonal structure. (**b,c**) Under the influence of spin-orbit coupling, the Mn orbitals take a uniaxial symmetry, the principal axis of the electron distribution becoming the moment direction. Owing to anisotropy in interfacial hybridization, the tunnel current, in a stack made of two Mn_2Au layers separated by a tunnel barrier, will depend on whether the directions of the AFM moments are identical (**b-b** or **c-c**) or perpendicular (**b-c**).

interfacial hybridization, the tunnel current will depend on whether the directions of the AFM moments are the same in both layers or arranged at 90° to each other.

In all TAMR structures developed to date, the tunnel magnetoresistance was found to decrease rapidly with increasing temperature and this was tentatively related to the degradation of the ordered magnetic state, which is the source of the TAMR signal[2,6]. The large exchange interactions required to preserve close-to-ground-state properties above room temperature, are present in Mn_2Au, which is among the materials having the highest magnetic ordering temperature. Mn_2Au appears to optimally combine all the required properties for becoming a cornerstone of future AFM spintronic devices.

Methods

Sample preparation and characterization. An ingot of Mn_2Au was prepared by induction melting and annealed for 3 days at 650 °C, below the peritectic temperature of 680 °C, at which the Mn_2Au phase decomposes. The annealed sample was ground into powder with a typical particle size of 5 μm and, after being sealed in a quartz tube, it was annealed at 350 °C for 1 h to remove strain induced by grinding.

X-ray diffraction. A detailed X-ray diffraction pattern was taken using Cu radiation ($\lambda_{Cu} = 1.54$ Å). An excellent fit to the known $MoSi_2$-type tetragonal structure of Mn_2Au was obtained using Rietveld analysis (FULPROF software; Supplementary Table S1)[11]. Impurity reflections were detected, arising from MnAu. The weight fraction of MnAu in the sample, derived from quantitative phase analysis of the diffraction pattern, is 2.5(4)%. The possible occupancy of Au sites by Mn atoms converged to a value of 3 (3)%, of which the difference from zero is not statistically significant.

Magnetometry. The DC susceptibility was measured using a Quantum Design VSM-SQUID, in fields up to 7 T and in the temperature range of 2–400 K. Two types of measurements were performed, either with the Mn_2Au powder free in the sample holder or embedded in an epoxy resin. Both types of measurements gave identical results.

NMR. The NMR experiment was performed on a home-built heterodyne spectrometer using standard spin-echo techniques. The frequency was scanned between 80 and 275 MHz. The ^{55}Mn spectrum was obtained by combining Fourier transforms of the spin-echo signal recorded for regularly spaced frequency values.

Neutron diffraction. The neutron diffraction study was performed on the D1B diffractometer at the Institut Laue-Langevin (Grenoble, France). A neutron wavelength of 1.28 Å was used. At this wavelength, the neutron flux is eight times less intense than at 2.52 Å. However, the Ewald sphere contains a larger volume of the reciprocal space and there is no $\lambda/2$ contamination. Neutron diffraction patterns were recorded at temperatures $T = 2$, 20, 300 550 700, 800 and 900 K.

The neutron diffraction pattern recorded at 2 K revealed that two main impurities are present in the sample: MnAu amounting to 2.3% of the total sample and MnO amounting to 0.4% (see Supplementary Fig. S1).

The 2 K pattern was initially analysed under the assumption that no magnetism is present in Mn_2Au, that is, only nuclear scattering is involved (Fig. 4a). The diagram calculated within FULPROF displays all experimentally observed reflections[11]. However, at low scattering angles, the experimental intensities of almost all reflections are larger than the calculated ones, and the discrepancy may be larger than the statistical error by up to three orders of magnitude. This suggests the existence of magnetic contributions to the Bragg reflections, with a magnetic structure described in the same cell as the crystallographic one, that is, a propagation vector equal to [000].

The neutron diffraction pattern was thus compared with each of the patterns expected for the magnetic structures allowed by group theory within the tetragonal structure of Mn_2Au. Of these, two are AFM ($\Gamma2$ and $\Gamma10$) and they were carefully examined. The fit corresponding to the $\Gamma2$ structure is shown in Fig. 4b (the structure is shown in the inset), whereas the one corresponding to $\Gamma10$ is shown in Fig. 3. Only the latter structure ($\Gamma10$) is compatible with the experimental data.

The high-temperature transformation of Mn_2Au into MnAu and γ-Mn was followed by collecting a series of short-duration neutron diffraction patterns, as the sample was slowly heated from 900 to 1,000 K. This is not of direct relevance for the present study and is not described in further detail in this paper.

References

1. Gould, C. *et al.* Tunneling anisotropic magnetoresistance: a spin-valve-like tunnel magnetoresistance using a single magnetic layer. *Phys. Rev. Lett.* **93**, 117203 (2004).

2. Park, B. G. *et al.* Tunneling Anisotropic magnetoresistance in multilayer (Co/Pt)/AlOx/Pt structures. *Phys. Rev. Lett.* **100**, 087204 (2008).
3. Shick, A. B., Khmelevskyi, S., Mryasov, O. N., Wunderlich, J. & Jungwirth, T. Spin-orbit coupling induced anisotropy effects in bimetallic antiferromagnets: A route towards antiferromagnetic spintronics. *Phys. Rev. B* **81**, 212409 (2010).
4. Wadley, P. *et al.* Tetragonal phase of epitaxial room-temperature antiferromagnet CuMnAs. *Nat. Commun.* **4**, 2322 (2013).
5. Wu, H.-C. *et al.* Mn_2Au: body-centered-tetragonal bimetallic antiferromagnets grown by molecular beam epitaxy. *Adv. Mater.* **24**, 6374–6379 (2012).
6. Park, B. G. *et al.* A spin-valve-like magnetoresistance of an antiferromagnet based tunnel junction. *Nat. Mater.* **10**, 347–351 (2011).
7. Meyer, A. J. P. Magnétisme des composés définis du système Mn-Au. *J. Phys. Rad.* 20, 430–434, 1959).
8. Abe, S. *et al.* Magnetic properties of ordered alloy AuMn2. *J. Magn. Magn. Mater.* **140-144**, 103–104 (1995).
9. Khmelevskyi, S. & Mohn, P. Layered antiferromagnetism with high Neel temperature in the intermetallic compound Mn_2Au. *Appl. Plys. Lett.* **93**, 162503 (2008).
10. Yamada, Y. & Sakata, A. An analysis method of antiferromagnetic powder patterns in spin-echo NMR under external fields. *J. Phys. Soc. Jpn* **55**, 1751–1758 (1986).
11. Rodriguez-Carvajal, J. Recent advances in magnetic structure determination by neutron powder diffraction. *Physica B* **192**, 55–69 (1993).
12. Bertaut, E. F. Representation analysis of magnetic structures. *Acta Cryst. A* **24**, 217–231 (1968).
13. Wills, A. S. A new protocol for the determination of magnetic structures using simulated annealing and representational analysis (SARAh). *Physica B* **276-278**, 680–681 (2000).
14. Tomeno, I., Fuke, H. N., Iwasaki, H., Sahashi, M. & Tsunoda, Y. Magnetic neutron scattering study of ordered Mn_3Ir. *J. Appl. Phys* **86**, 3853–3856 (1999).
15. Pal, L., Kren, E., Kadar, G., Szabo, P. & Tarnoczi, T. Magnetic structures and phase transformations in Mn based CuAuI type alloys. *J. Appl. Phys* **39**, 538–544 (1968).
16. Blundell, S. J. *et al.* Detection of magnetic order in the $S = 1$ chain compound $LiVGe_2O_6$ using implanted spin-polarized muons. *Phys. Rev. B* **67**, 224411 (2003).
17. Kuz'min, M. D. Shape of temperature dependence of spontaneous magnetization of ferromagnets: quantitative analysis. *Phys. Rev. Lett.* **94**, 107204 (2005).
18. Kawakami, M., Kasamatsu, Y. & Ido, H. Temperature and pressure dependence of NMR frequencies in ferromagnetic Heusler alloys containing cobalt and manganese. *J. Magn. Magn. Mater.* **70**, 265–267 (1987).
19. Yoshimura, K., Shiga, M. & Nakamura, Y. NMR study of magnetic state of RMn_2 intermetallic compounds. II R = heavy rare-earths. *J. Phys. Soc. Jpn* **55**, 3585–3595 (1986).
20. O'Grady, K., Fernandez-Outon, L. E & Vallejo-Fernandez, G. A new paradigm for exchange bias in polycrystalline thin films. *J. Magn. Magn. Mater* **322**, 883–899 (2010).
21. Akulov, N. S. Zur Quantentheorie der Temperaturabhängigkeit der Magnetisierungskurve. *Z. Physik* **100**, 197–202 (1936).

Author contributions

V.M.T.S.B. and D.G. proposed the study; V.M.T.S.B. prepared the samples; C.V.C. performed the X-ray analysis; V.M.T.S.B., C.V.C. and D.G. performed the magnetic measurements; V.M.T.S.B., C.V.C. and D.G. performed the neutron experiments; C.V.C. performed the neutron data analysis; NMR experiment: M.-H.J. and H.M. performed the NMR experiments; all authors discussed the paper; D.G. and M.-H.J. pepared the manuscript with input from all authors.

Additional information

Supplementary Information accompanies this paper at http://www.nature.com/naturecommunications

Competing financial interests: The authors declare no competing financial interests.

Reprints and permission information is available online at http://npg.nature.com/reprintsandpermissions/

How to cite this article: Barthem, V.M.T.S. *et al.* Revealing the properties of Mn_2Au for antiferromagnetic spintronics. *Nat. Commun.* 4:2892 doi: 10.1038/ncomms3892 (2013).